

## **Supplementary Information: Transformation of Sintered CsPbBr<sub>3</sub> Nanocrystals to Cubic CsPbI<sub>3</sub> and Gradient CsPbBr<sub>x</sub>I<sub>3-x</sub> Through Halide Exchange.**

Jacob B. Hoffman, A. Lennart Schleper<sup>‡</sup>, and Prashant V. Kamat\*

Radiation Laboratory

University of Notre Dame

Notre Dame, IN 46556, United States

---

\* Corresponding author: Prashant V. Kamat ([pkamat@nd.edu](mailto:pkamat@nd.edu))

<sup>‡</sup> Present Address: University of Heidelberg, Germany

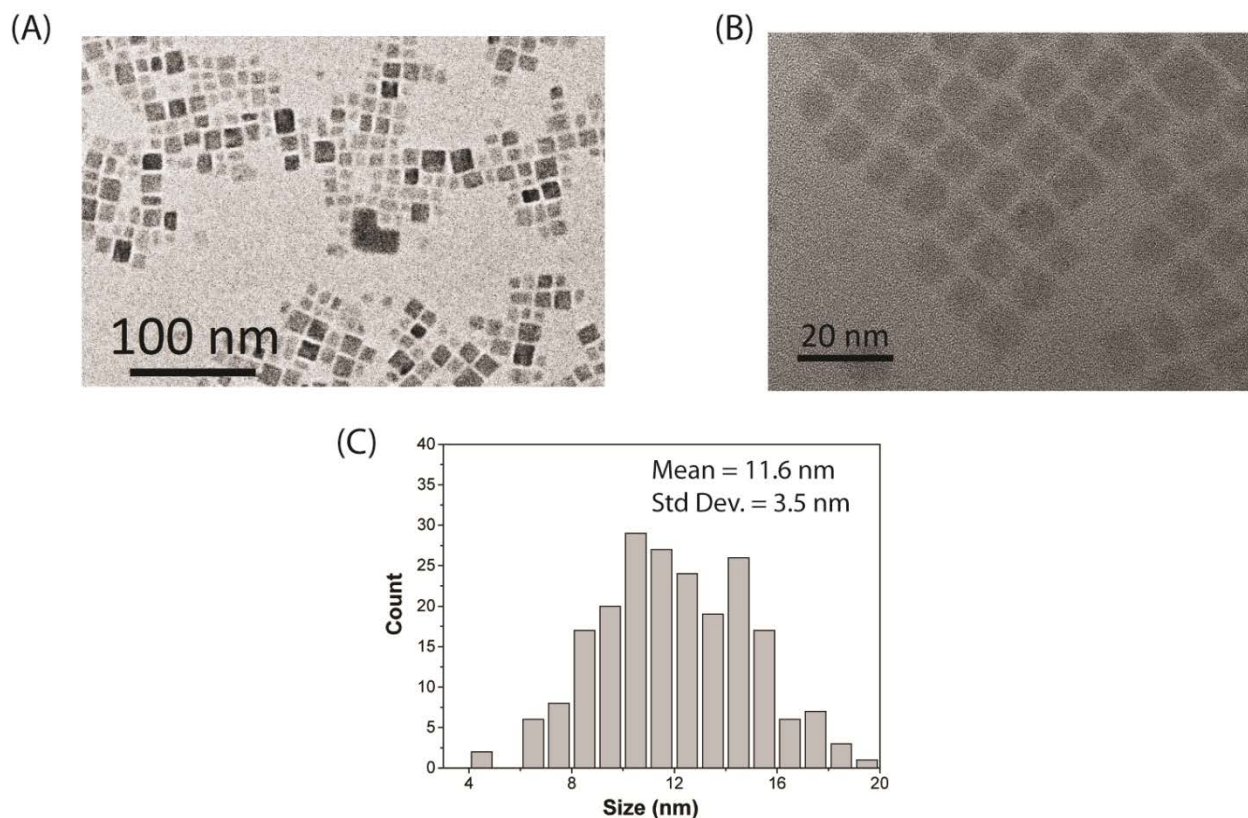


**Figure S1:** TEM images of CsPbBr<sub>3</sub> NCs post-cleaning on (A) 100 nm and (B) 20 nm scales. (C) Size distribution of NCs, showing an average size of 11.6 nm with a standard deviation of 3.5 nm. Despite a small FWHM (19 nm) observed for nanocrystal photoluminescence, the size distribution was relatively broad.

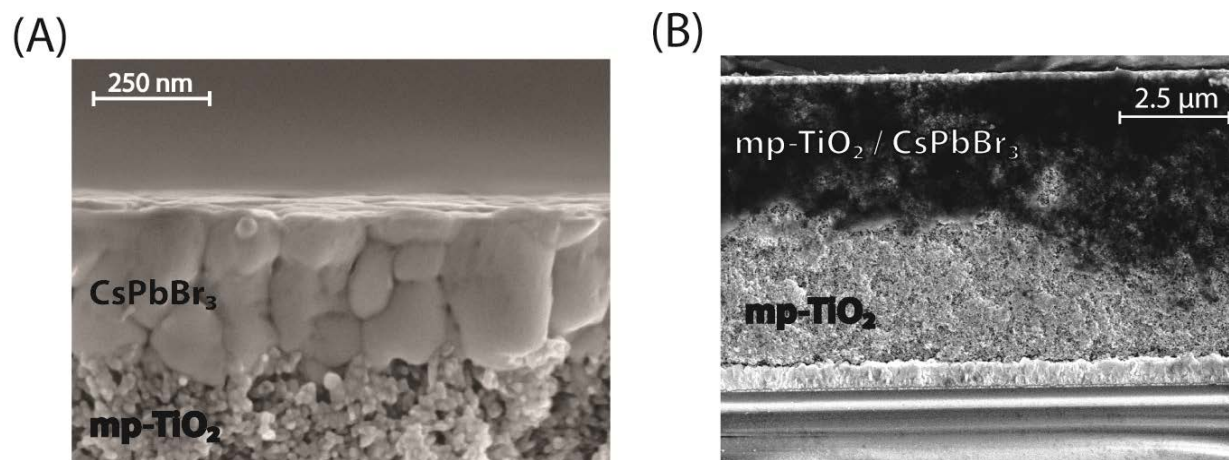


**Figure S2:** Cross sectional SEM images of (A) spin casted CsPbBr<sub>3</sub> on a mesoporous TiO<sub>2</sub> substrate and (B) drop casted CsPbBr<sub>3</sub> on a thicker mesoporous TiO<sub>2</sub> substrate. Drop casted CsPbBr<sub>3</sub> permeated into the mesoporous TiO<sub>2</sub> as evidenced by the contrast between mp-TiO<sub>2</sub> (bright) and mp-TiO<sub>2</sub> / CsPbBr<sub>3</sub> (dark) layers. In the spin casted sample the TiO<sub>2</sub> layer remained bright,

indicating CsPbBr<sub>3</sub> did not permeate into the mesoporous structure, and instead agglomerated on the substrate surface.

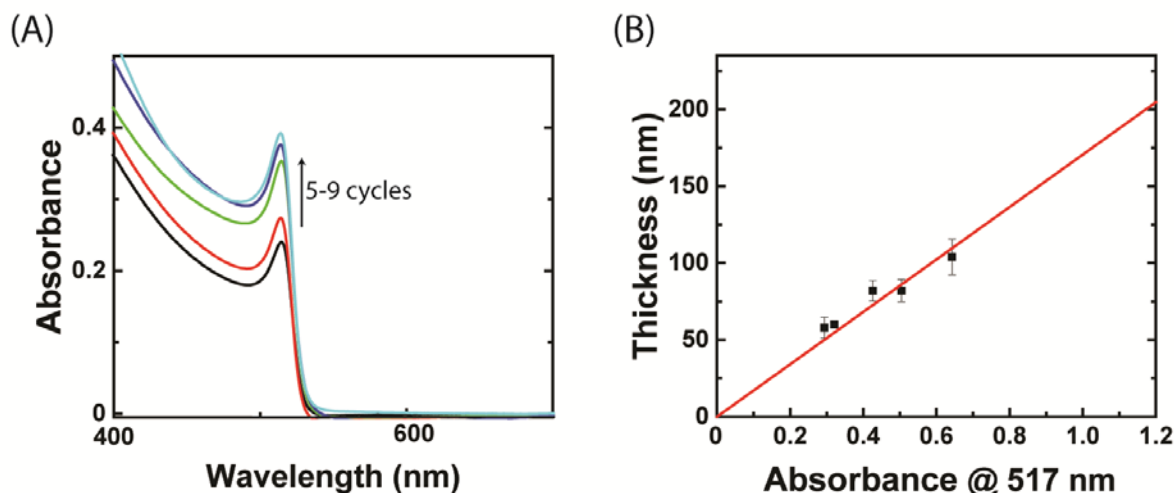


**Figure S3:** (A) Absorbance of CsPbBr<sub>3</sub> films upon glass substrates for 5-9 deposition cycles. Spectra were obtained using a Jasco V-670 spectrophotometer equipped with an integrating sphere. This instrument was used in place of the Cary-50 bio spectrophotometer described in the main text to correct for spectral and diffuse reflectance. (B) Film thickness vs. absorbance at 517 nm (peak) for the same films found *via* a Bruker DektakXT profilometer. The linear trend shows that NC deposition is controllable with increasing thickness upon deposition of multiple cycles.

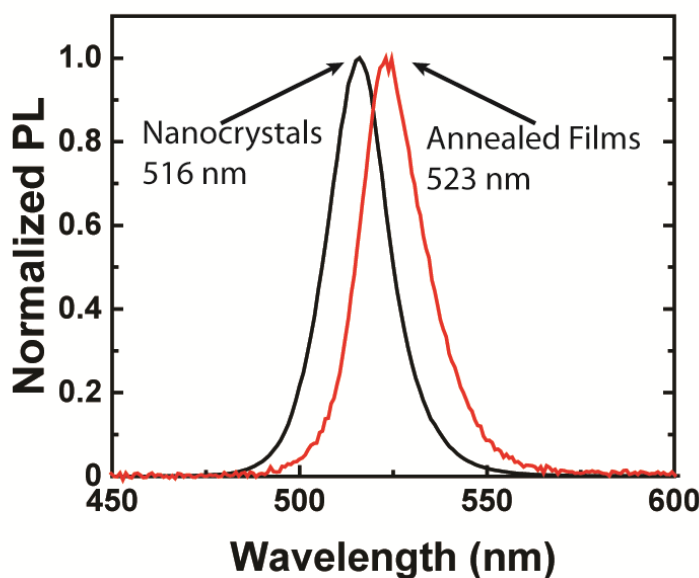


**Figure S4:** Normalized photoluminescence (PL) of CsPbBr<sub>3</sub> for NCs in solution and post annealed films. NCs emission was acquired using Horiba fluorolog-3 as described in the main text. Film PL

was acquired using an ocean optics QE pro spectrophotometer with 365 nm excitation. Similar to absorption, PL redshifted, indicating a change from quantum confined NCs to bulk crystallites.

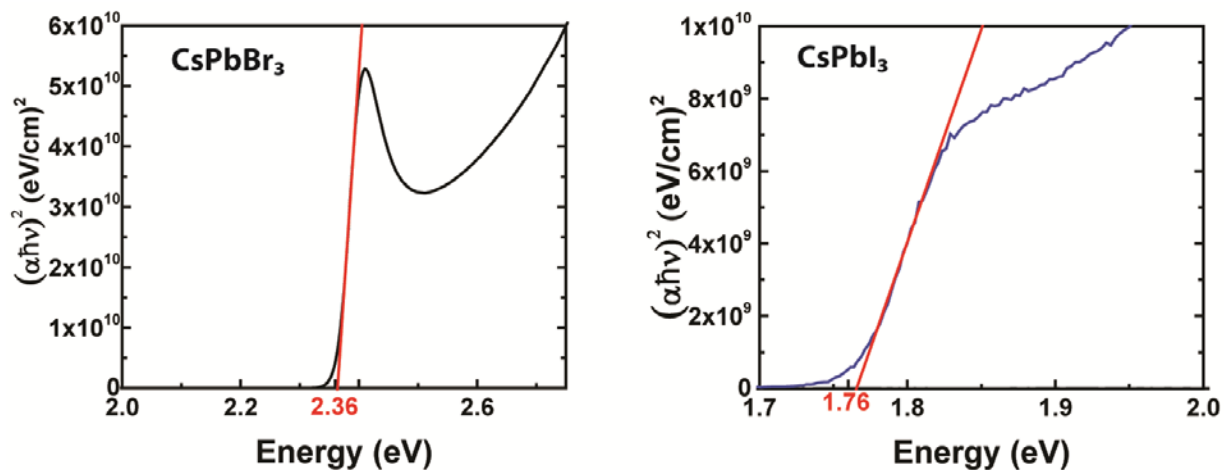


**Figure S5:** Tauc plots of CsPbBr<sub>3</sub> and fully exchanged CsPbI<sub>3</sub> films (50 nm). Direct bandgaps were found to be 2.36 eV and 1.76 eV for CsPbBr<sub>3</sub> and CsPbI<sub>3</sub> respectively.

73 grain boundaries in 8  $\mu\text{m}$

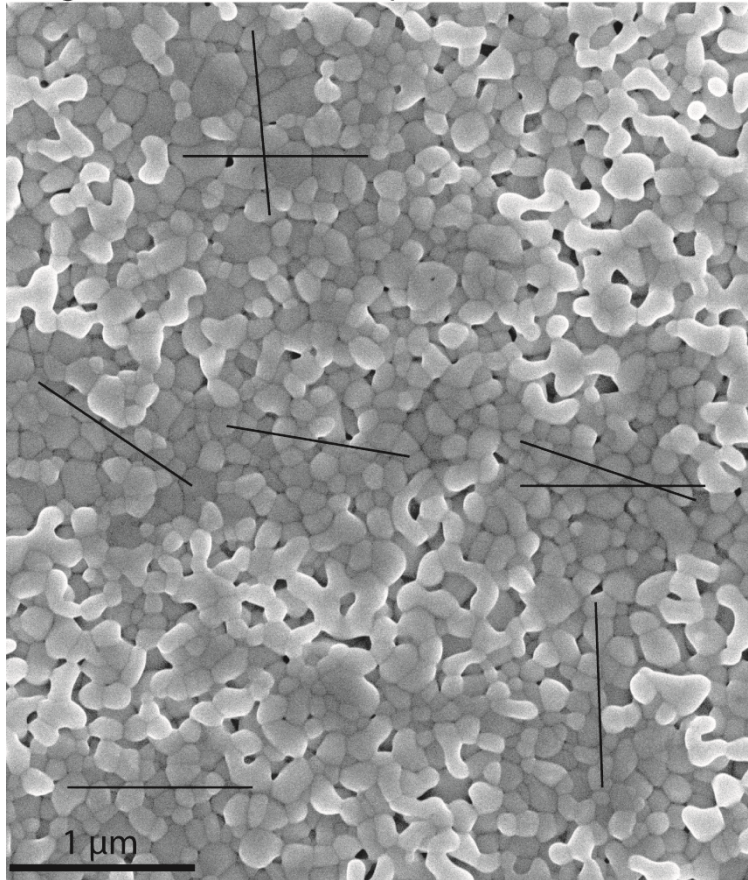


**Figure S6:** Average grain diameter was found using the intercept method. Lines were drawn across a top down SEM image equating to 8  $\mu\text{m}$  total distance. The number of intercepts between grains for all lines were counted. The average grain size was then found through the expression,  $\left(\frac{\text{total number of intercepts}}{\text{total distance}}\right)$ . The analysis was repeated three times to find an average diameter of  $112 \pm 2.5 \text{ nm}$ .

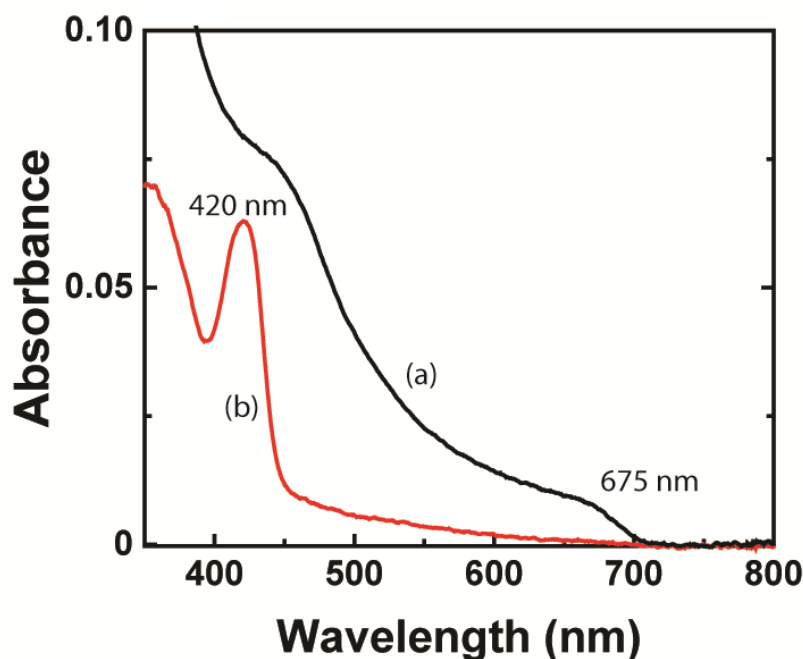


**Figure S7:** Direct deposition of CsPbI<sub>3</sub> NCs onto a TiO<sub>2</sub> substrate following the methods described in the text. **(a)** Before annealing the NCs kept a cubic crystal structure, featuring an absorbance peak at 675 nm (consistent with solution). During annealing visible absorbance was lost **(b)**, and an absorption peak at 420 nm appeared. The appearance of this high energy absorption peak is consistent with formation of bulk orthorhombic CsPbI<sub>3</sub> which has a bandgap of 3.01 eV (410 nm).

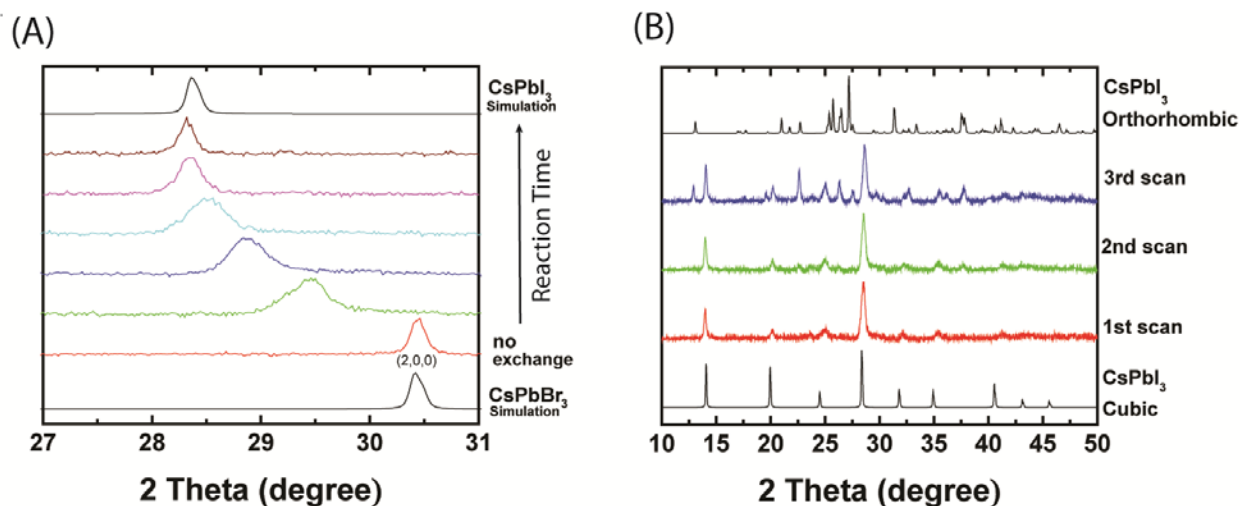


**Figure S8:** **(A)** Figure 2B zoomed in on the diagnostic (2,0,0) peak. Peak broadening followed by subsequent re-sharpening suggests that there is a distribution of CsPbBr<sub>x</sub>I<sub>3-x</sub> present in the film. **(B)** Films soaked past 7 minutes begin to degrade into the orthorhombic phase under ambient conditions. This is reflected in orthorhombic CsPbI<sub>3</sub> peaks growing in over subsequent XRD scans. By the third scan the orthorhombic phase was prominent, and the film was white in color. This is likely tied to humidity as films would degrade into the orthorhombic phase on the benchtop, but were indefinitely stable under dry conditions.

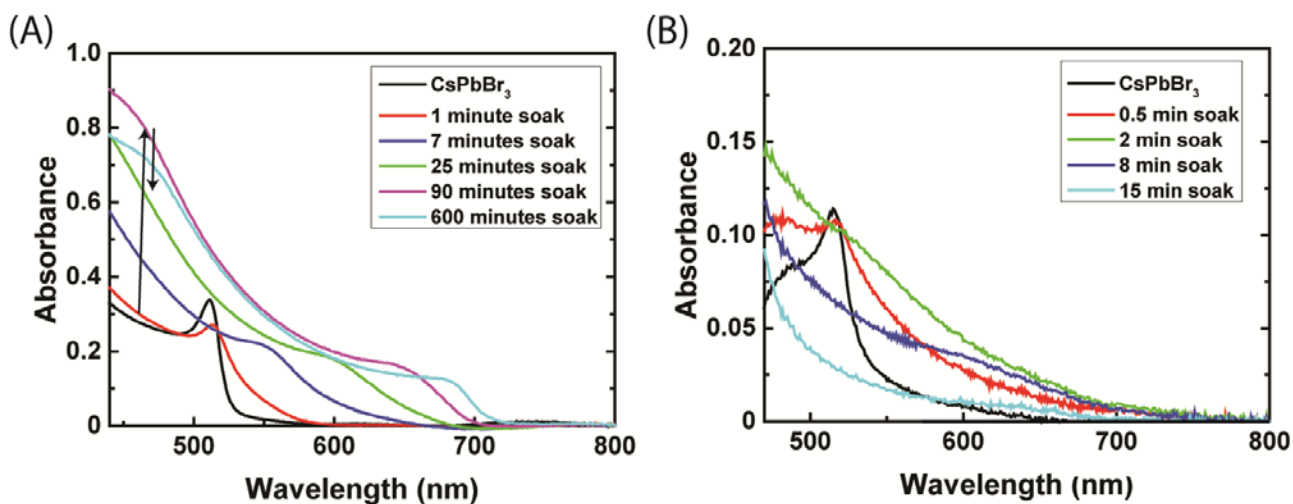
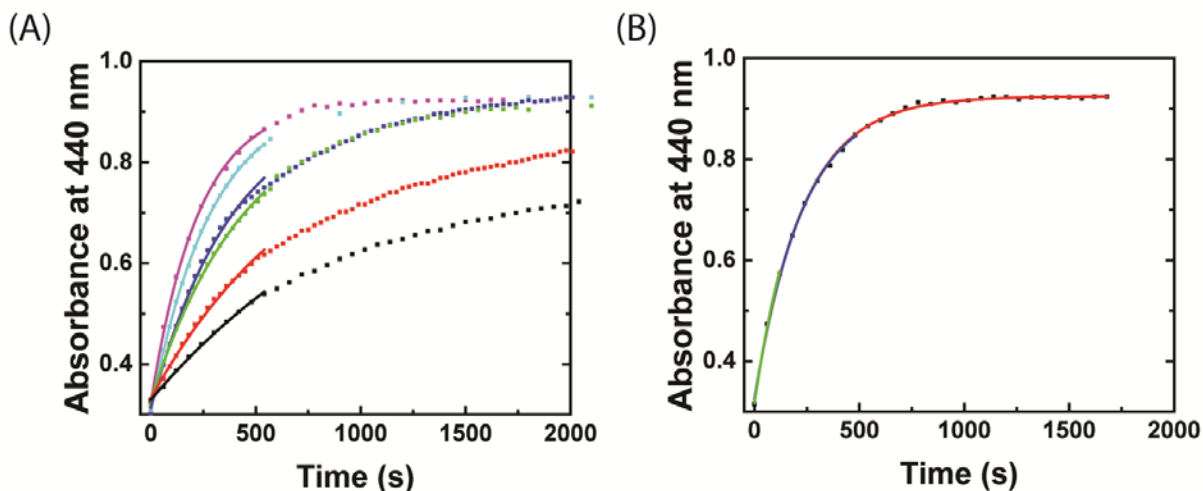


**Figure S9: (A)** *In situ* halide exchange reaction of CsPbBr<sub>3</sub> soaked in a PbI<sub>2</sub> solution at 65 °C. The initial increase in absorbance was convoluted with a decrease in absorbance at long reaction times. This was attributed to film etching from excess oleic acid and oleylamine coordinating to Cs<sup>+</sup> and Pb<sup>2+</sup> cations. **(B)** We confirmed this effect by soaking a CsPbBr<sub>3</sub> film in a solution of half OAc and half OAM at 65 °C. The film completely dissolved within 15 minutes of soaking, showing the connection between excess ligands and the absorbance decrease.



Soaking Temp (°C)	A	k	y <sub>0</sub>	R <sup>0</sup>
94 (Magenta)	0.59	0.0044 ± 0.0001	0.92	0.99
79 (Cyan)	0.62	0.0035 ± 0.0001	0.92	0.99
75 (Blue)	0.61	0.0026 ± 0.0001	0.92	0.99
70 (Green)	0.59	0.0022 ± 0.0001	0.92	0.99
64 (Red)	0.59	0.0013 ± 0.0001	0.92	0.99
56 (Black)	0.59	0.0008 ± 0.0001	0.92	0.99

Data Range	A	k	y <sub>0</sub>	R <sup>0</sup>
Full Range (Red)	0.60	0.0043 ± 0.0001	0.92	0.99
500 seconds (Blue)	0.60	0.0044 ± 0.0001	0.92	0.99
125 seconds (Green)	0.60	0.0047 ± 0.0001	0.92	0.99

**Figure S10: (A)** Fitting of the halide exchange reaction at various soaking solution temperatures. The data was fit to a monoexponential equation of the form  $y = Ae^{xk} + y_0$ , where A is a fitting amplitude, k is the pseudo first order rate constant, and  $y_0$  is a fitting offset. At temperatures below 79 °C the rise in absorbance from the halide exchange reaction was convoluted with a

decrease in absorbance from film etching, due to excess ligands in the soaking solution. This convolution led to poor fittings at low temperatures. Thus, we fit the data only using the first 500 s of data and fixed the offset to 0.92, before film etching significantly contributed to overall absorbance. This offset was the endpoint of the halide exchange reaction (obtained from 94 and 79 °C full fittings) and was assumed to stay constant for all exchange temperatures. Fitting the absorbance data with fewer points did not significantly change the obtained fits. To show this, the 94 °C exchange data was fit with three data ranges: Full (red), 500 seconds (blue), and 125 seconds (green) **(B)**. There was no significant difference between the fits when amplitude was fixed to 0.92 (as shown in the table).

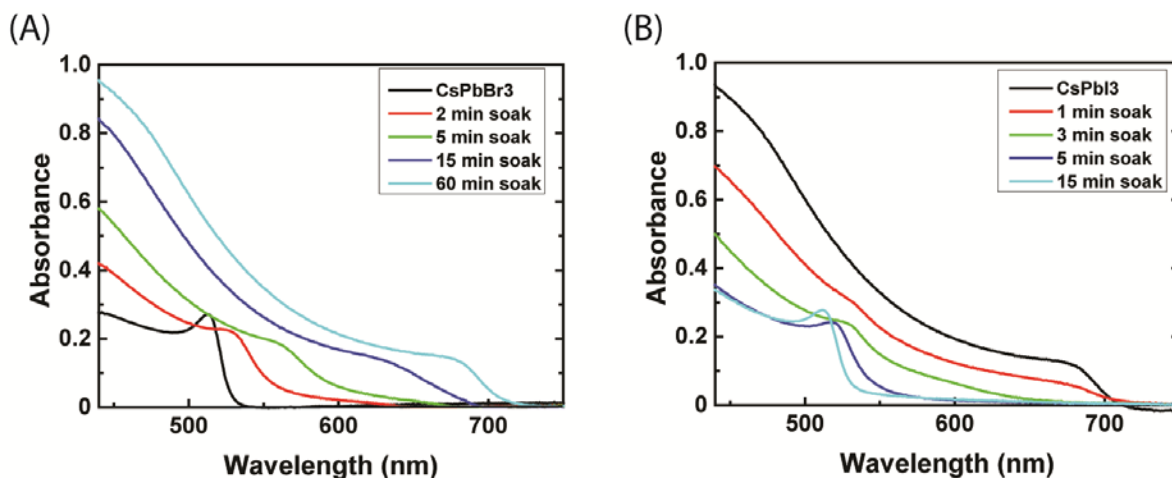


**Figure S11:** The halide exchange reaction was found to be reversible by switching the PbI<sub>2</sub> soaking solution with a PbBr<sub>2</sub> soaking solution. **(A)** shows the forward exchange at 75 °C for a 25 nm thick film. The reversibility is shown in **(B)** where the same exchanged film was placed in a PbBr<sub>2</sub> soaking solution. The reverse exchange reaction (Br<sup>-</sup> to I<sup>-</sup>) proceeded approximately four times faster than forward direction at the same temperature and film thickness. This faster exchange indicated that smaller bromide anions required less energy to be inserted into the film.

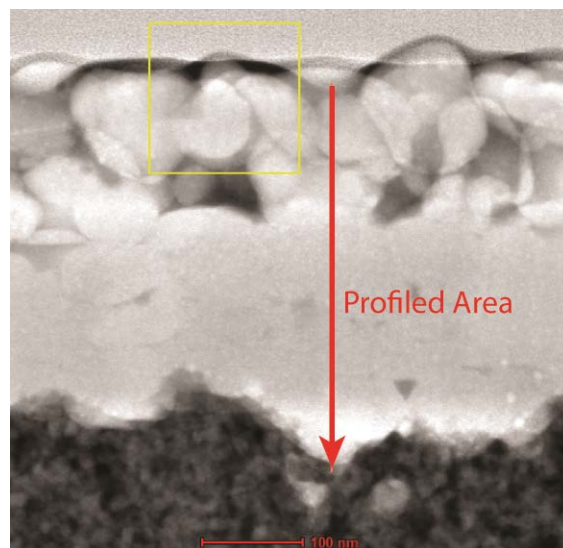
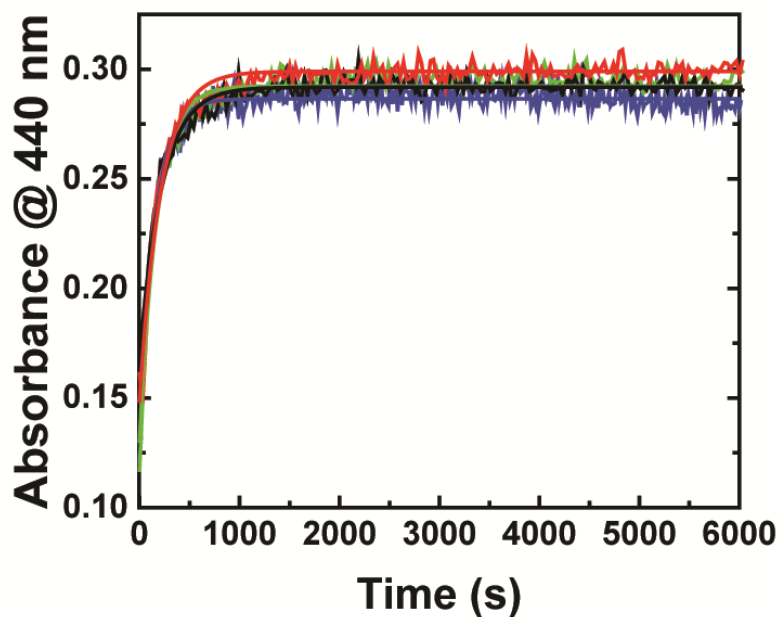


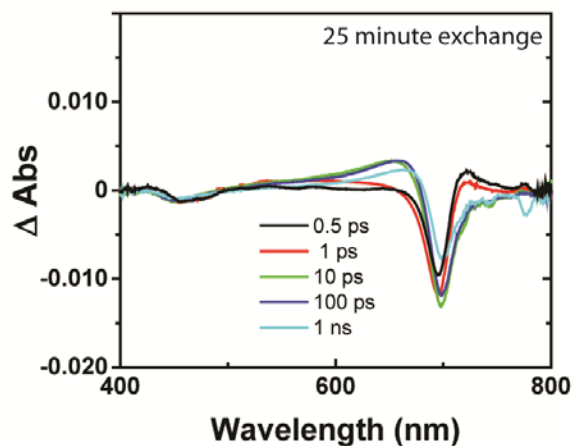
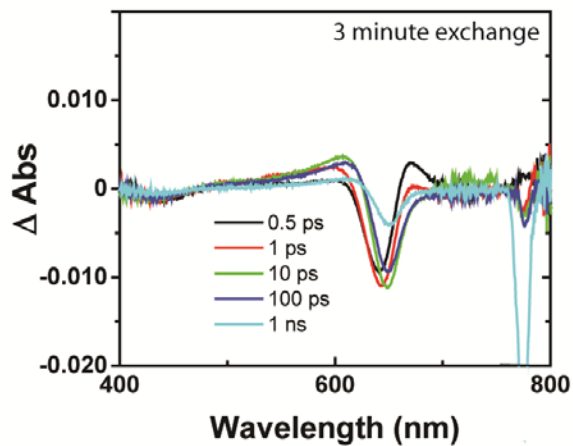
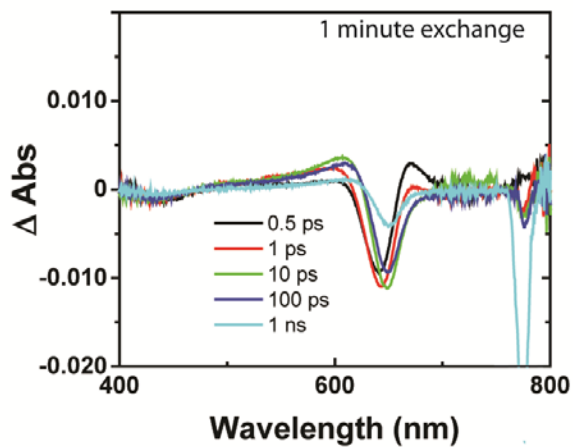
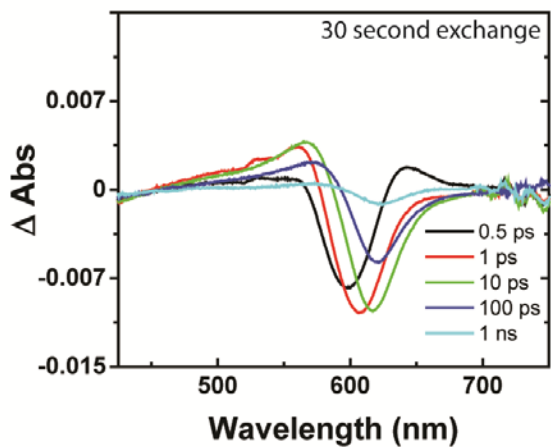
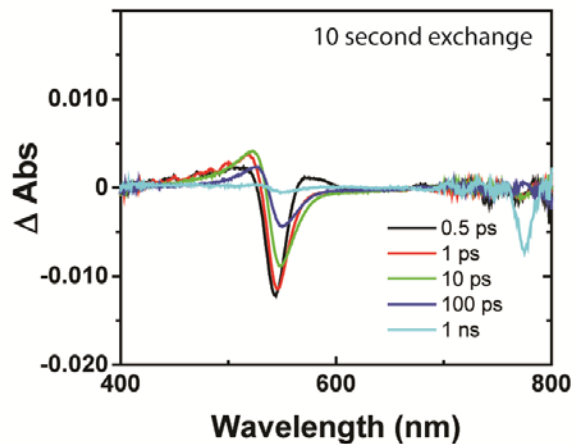
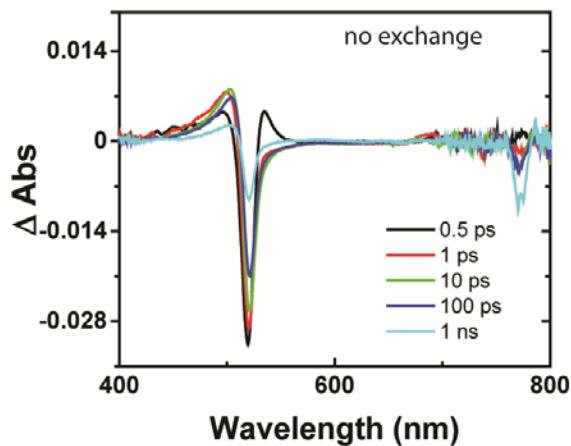
**Figure S12:** Cross sectional STEM image of the 30 minute exchanged 350 nm film used for elemental analysis. The red line represents the area used in the EDX experiment to profile the film composition as a function of film depth.



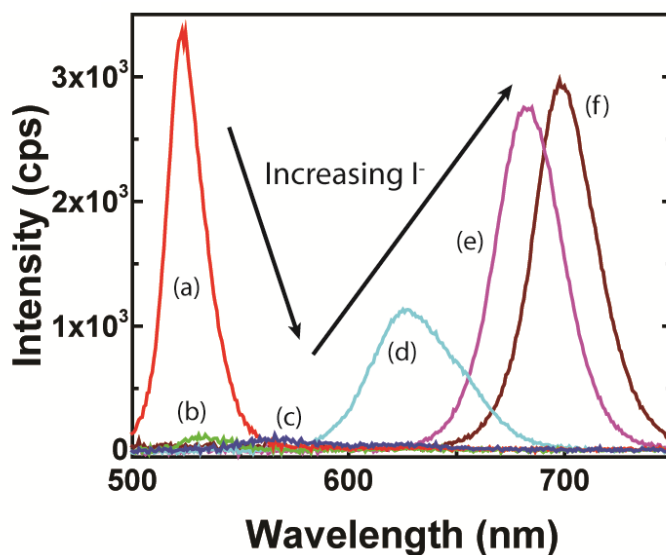
Iodide Concentration	A	y0	k	R0
7.5 mM (half) (red)	-0.15	0.30	0.0048	0.93
14 mM (normal) (black)	-0.15	0.29	0.0056	0.89
28 mM (double) (green)	-0.15	0.29	0.0052	0.90
56 mM (quadruple) (blue)	-0.15	0.29	0.0063	0.92

**Figure S13:** Monitored absorbance and monoexponential fits of halide exchange reactions using 25 nm thick films at 90 °C with varying iodide soaking solution concentrations. Fittings obtained

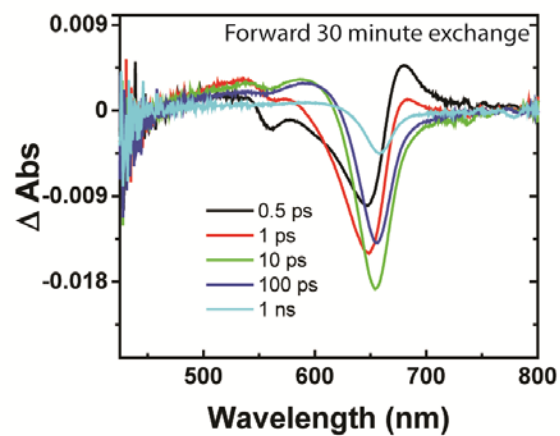
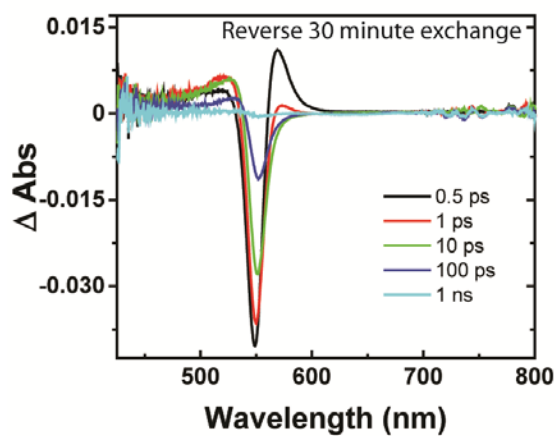
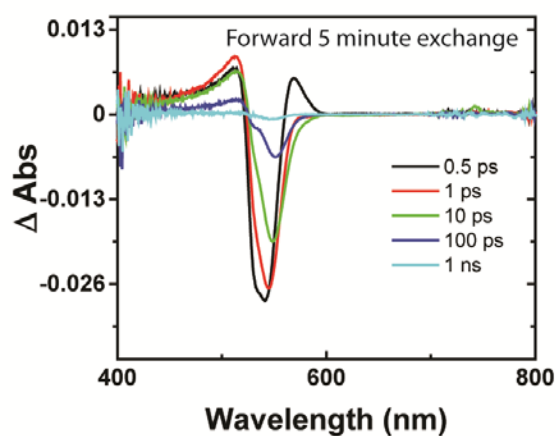
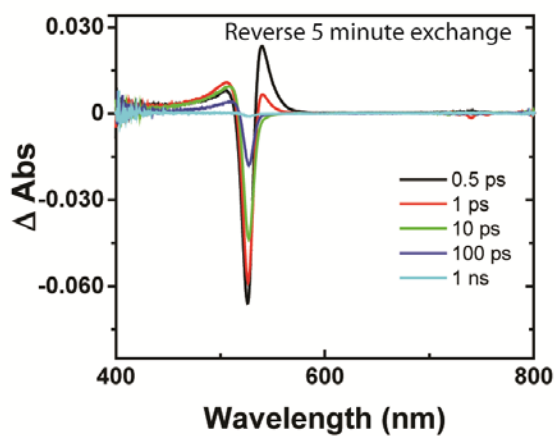
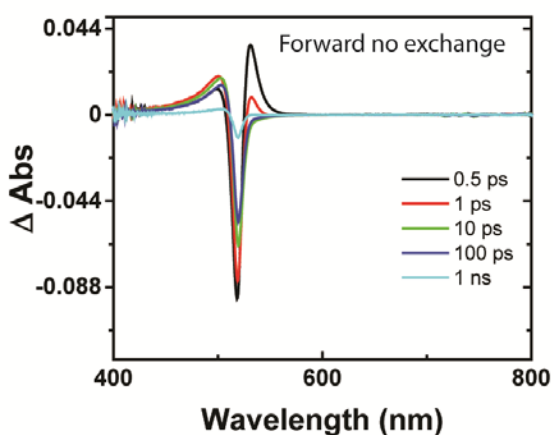
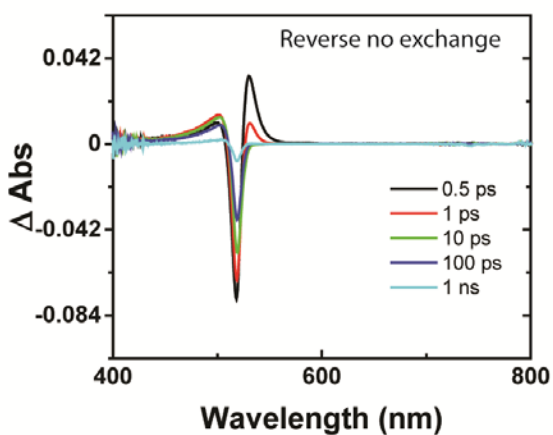
for iodide concentrations between 7.5 mM to 56 mM showed no significant difference in the obtained pseudo first order reaction rate constants. Thus, we conclude that iodide diffusion to the film surface did not limit halide exchange.



**Figure S14:** Difference absorption spectra of 25 nm films at various exchange times. Such thin films were used to ensure minimal compositional differences. However, there was some broadening for the 30 second sample indicating the presence of slight compositional differences.



**Figure S15:** Photoluminescence spectra of (a) CsPbBr<sub>3</sub> and exchanged films with increasing iodide content (b-f). With increased iodide content photoluminescence redshifted similar to the trend observed in absorption spectra. Additionally, photoluminescence initially decreased with small amounts of iodide introduced, later recovering at longer soaking times. This trend in photoluminescence matched the trend of bleach recovery in transient absorption experiments. Film photoluminescence was acquired using an ocean optics QE pro spectrophotometer with 365 nm excitation.



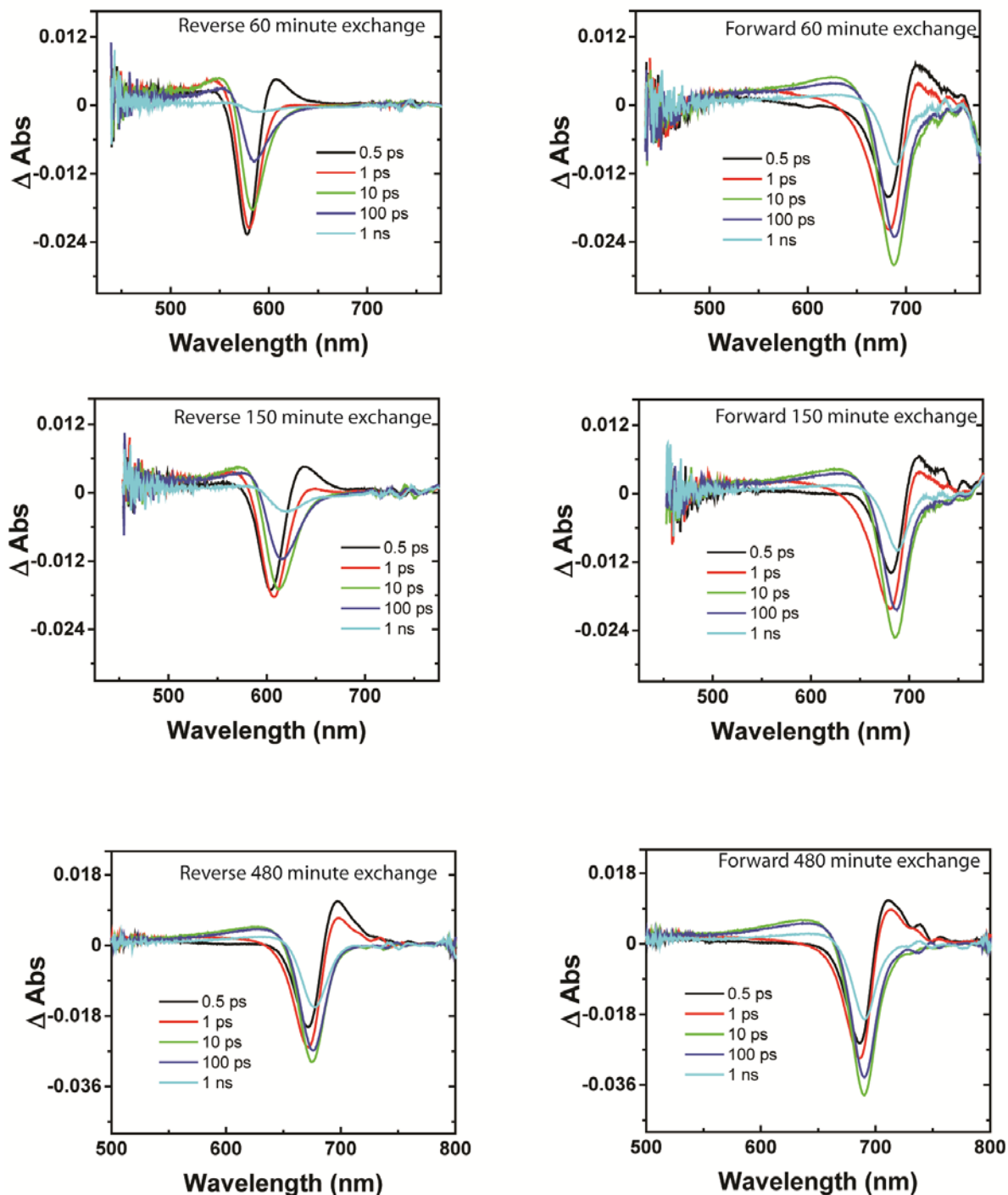


**Figure S16:** Complete difference absorption spectra of exchanged 350 nm films (steady state absorption in figure 4) for reverse and forward excitation. The large differences in forward vs. reverse excitation show the major variation in film composition at different film depths. Excitation of the compositional gradient did not exhibit as broad of a bleach as the 15 min exchanged sample (in main text) due to the limited penetration depth of the 387 nm pump.

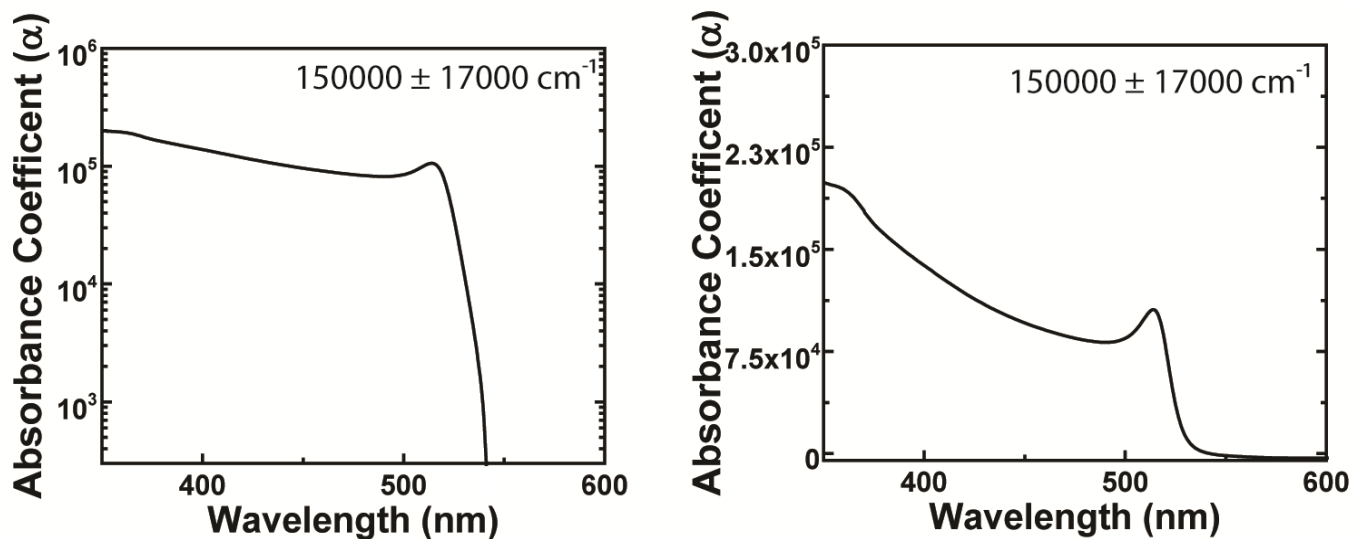
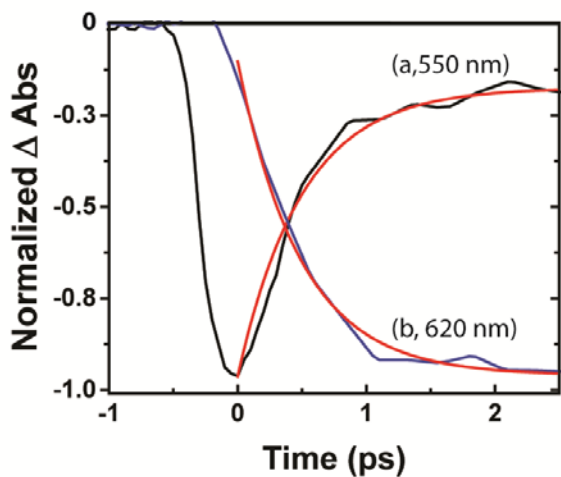


**Figure S17:** The absorbance coefficient ( $\alpha$ ) of pure CsPbBr<sub>3</sub> was found using the expression,  $\alpha = \frac{\ln(10)A}{x}$ , where A is the film absorbance and x is pathlength (film thickness). Using the data in Figure S3, the absorbance coefficient was found to be 150,000  $\pm$  17,000 cm<sup>-1</sup> at 387 nm, the wavelength of the transient absorption pump. An estimation of pump penetration depth was obtained from the inverse of the absorbance coefficient to be 66.6 nm.



Wavelength (nm)	A	y <sub>0</sub>	τ	R <sub>0</sub>
550 (black)	0.89	-0.18	-0.49 ± 0.02	0.99
620 (blue)	-0.82	-1	0.5 ± 0.02	0.98

**Figure S18:** Monoexponential fits of difference absorption kinetics at 550 nm (black) and 620 nm (blue) for the 350 nm film exchanged for 15 minutes at 120 °C (featured in Figures 6B and 7A). At 550 nm the difference absorption featured an ultrafast decay that corresponded to a growth at

620 nm after pump excitation. Time zero was shifted -0.5 ps to align with the bleach maximum at 550 nm. This shift was done to avoid contributions from pump excitation contributing to the fit. The fitting equation was  $y = Ae^{x/\tau} + y_0$  where the parameters are the same as Figure S10 with the exception of the time constant ( $\frac{1}{\tau}$ ) replacing the rate constant (k). The obtained time constants were -0.49 and 0.5 ps for the decay and growth components respectively, signifying a connection between the two processes.